Materials & Design 229 (2023) 111878

Contents lists available at ScienceDirect

Materials & Design

journal homepage: www.elsevier.com/locate/matdes

A data-driven model of the yield and strain hardening response of commercially pure titanium in uniaxial stress

Burcu Tasdemir [a], Vito Tagarielli [b,*], Antonio Pellegrino [a,*]

[a] Department of Engineering Science, University of Oxford, Oxford, UK
[b] Department of Aeronautics, Imperial College London, London, UK

HIGHLIGHTS

- Random experiments are designed to produce training data on the response of pure Titanium.
- A suitable architecture of a surrogate model is determined and the model is trained.
- The accuracy of the predictions of the surrogate models are evaluated and compared with those of an established theoretical model.

GRAPHICAL ABSTRACT

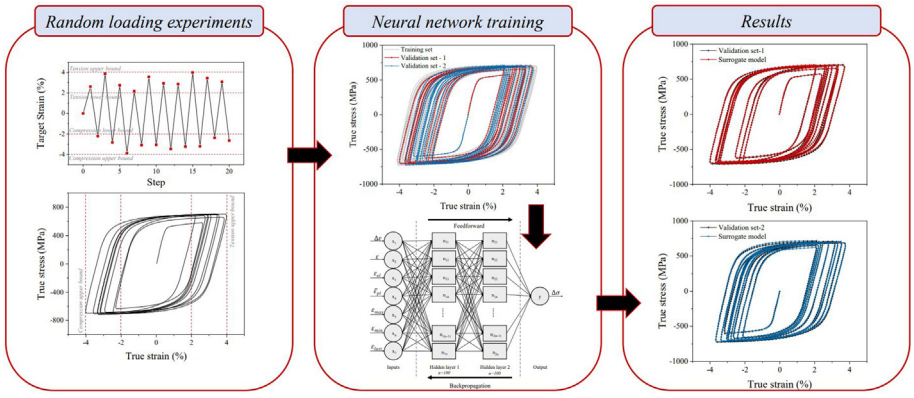

ARTICLE INFO

Article history:
Received 9 February 2023
Revised 4 March 2023
Accepted 26 March 2023
Available online 30 March 2023

Keywords:
Plasticity
Cyclic loading
Strain hardening
Machine learning
Surrogate model

ABSTRACT

This study presents a technique to develop data-driven constitutive models for the elastic-plastic response of materials, and applies this technique to the case of commercially pure titanium. The complex yield and strain hardening characteristics of this solid are captured for random non-monotonic uniaxial loading, without relying on specific theoretical descriptions. The surrogate model is obtained by supervised machine learning, relying on feed-forward neural networks trained with data obtained from random loading of titanium specimens in uniaxial stress. Uniaxial tests are conducted in strain control, applying random histories of axial strain in the range [−0.04, 0.04], to prevent the occurrence of significant damage. The corresponding stress versus strain histories are subdivided into a finite number of increments, and machine learning is applied to predict the change in stress in each increment. A suitable architecture of the data-driven model, key to obtaining accurate predictions, is presented. The predictions of the surrogate model are validated by comparing to experiments not used in the training process, and compared to those of an established theoretical model. An excellent agreement is obtained between the measurements and the predictions of the data-driven surrogate model.

1. Introduction

Accurate predictions of the elastic-plastic response of engineering materials are fundamental in structural design and failure analysis. For solids undergoing non-monotonic reversed loading,

* Corresponding authors.
E-mail addresses: v.tagarielli@imperial.ac.uk (V. Tagarielli), antonio.pellegrino@eng.ox.ac.uk (A. Pellegrino).

https://doi.org/10.1016/j.matdes.2023.111878
0264-1275/

involving the sequential application of positive and negative plastic strains, accurate predictions can only be obtained if the details of the strain-hardening characteristic of the material are adequately captured. The theoretical models available to engineers often rely on simplifying assumptions, such as purely isotropic or kinematic hardening, or combinations of these. In this study, we model the complex strain hardening of commercially pure titanium using exclusively the results of carefully designed measurements, by applying supervised machine learning.

Plastic deformation is a dissipative mechanism and is therefore history-dependent; several researchers have applied machine learning techniques to predict this phenomenon [1–4]. In the presence of repeated and reversed plastic deformation, as for example in cyclic plasticity, the implementation of accurate constitutive models is complicated by the complex history-dependent strain hardening response of solids, which has been explored extensively for some metallic alloys [5,6].

Machine learning is being applied to solid mechanics to accelerate or enable complex material design and optimisation, including constitutive models for multiphysics problems [7,8], identification of material properties [9,10], inverse modelling and predictions of plastic flow as a function of temperature and strain rate [11,12]. Machine learning was also used to extend the experimentally measurable range of strains and enhance springback predictions in [13]. Most of the published work focuses on monotonic loading, in which it is not necessary to accurately capture the yield and strain hardening characteristic of the material investigated. Several authors (for example [14–16]) applied machine learning techniques to the case of reversed plasticity, developing surrogate models trained on datasets generated numerically, in which simple strain hardening characteristics (isotropic hardening) were assumed. Kinematic hardening was successfully predicted by data-driven models obtained using numerically generated data in [17,18].

In this study, we use data from actual experiments in uniaxial stress to construct a constitutive model that captures the details of the yielding and strain hardening response of a commercially pure titanium. The proposed technique is in principle applicable to any solid, but commercially pure titanium is chosen here for its ready availability and its well-studied strain hardening response, displaying a clear Bauschinger effect. Below we use feed-forward Neural Networks (a neural network is abbreviated below by NN) to construct a rate-independent surrogate model, also independent of any theoretical assumptions on the details of the material's yield and strain hardening. We use the surrogate model to predict the stress history consequent to the application of a random strain history.

The paper is structured as follows. In Section 2 we illustrate the details of the experiments conducted, while Section 3 presents the implementation of the data-driven surrogate model; results are presented and discussed in Section 4.

2. Mechanical tests

2.1. Material and specimen geometry

Extruded bars of commercially pure titanium (Grade 3), of diameter 10 mm, were obtained from Smiths Metal Centres. Axisymmetric dogbone specimens were manufactured by turning, according to the geometry in Fig. 1. The specimen geometry was designed considering previous research work ([19–20]) on cyclic plasticity tests, to ensure approximately uniform stress and strain in the gauge portion and to prevent buckling in presence of compressive loading.

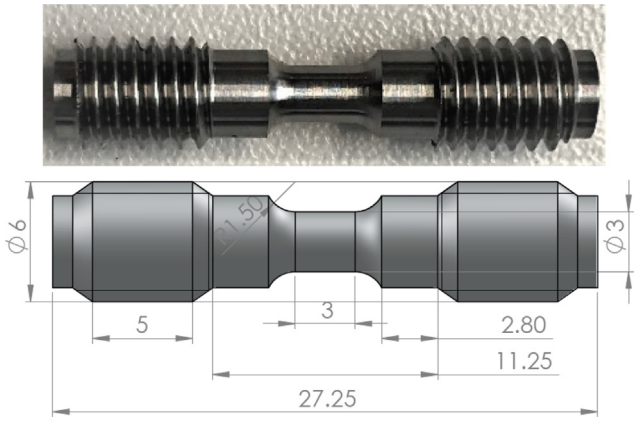

Fig. 1. Specimen geometry (all dimensions in mm).

2.2. Experimental setup and procedure

A portion of the specimen's gauge length was speckled to measure strain. The specimen was connected to a steel loading fixture by threaded connections. The fixture was loaded by a screw-driven testing machine via mounting pins, as shown in Fig. 2. Uniaxial tension–compression cyclic experiments were conducted in real-time strain control; a video extensometer was used to measure the axial strain in the gauge portion and a feedback loop controlled such strain imposing a constant nominal strain rate of $|\dot{\varepsilon}| = 10^{-3}\,\mathrm{s}^{-1}$ in all tests. The force was measured by a 20 kN resistive load cell. Strain and force measurements were recorded at a frequency of 10 Hz.

Nine random histories of reversed strain were imposed on different specimens. Each random history comprised 20 loading steps (10 cycles), and in each step a random change in axial strain $|\Delta\varepsilon_i| \in [\Delta\varepsilon_{\min}, \Delta\varepsilon_{\max}]$, $(i = 1, 2...20)$ was imposed on the specimen; the sign of the first change in strain was chosen randomly, while subsequent loading steps alternated positive and negative signs of the applied strain, i.e.

$$\begin{aligned} \Delta\varepsilon_{i=1} &= \mathrm{sign}(0.5 - r)[\Delta\varepsilon_{\min} + r(\Delta\varepsilon_{\max} - \Delta\varepsilon_{\min})]; \\ \Delta\varepsilon_i &= -\mathrm{sign}(\Delta\varepsilon_{i-1})[\Delta\varepsilon_{\min} + r(\Delta\varepsilon_{\max} - \Delta\varepsilon_{\min})], \end{aligned} \tag{1}$$

where r is a uniformly random number between 0 and 1. We chose $\Delta\varepsilon_{\min} = 0.02$ and $\Delta\varepsilon_{\max} = 0.04$ to ensure that the material displayed both elastic and elastic–plastic responses in each step (note that the initial yield strain of pure titanium is less than 1 %). The choice of having only 20 steps in each experiment was made to avoid low-cycle fatigue damage, as we will discuss quantitatively below. We note that some of the experiments were terminated before the 20th step, due to premature degradation of the speckling pattern during the test (and consequent inability to measure strain).

Fig. 3 illustrates a representative random strain history imposed in one of the experiments. Fig. 3 (a) shows the nominal strain versus time history, and Fig. 3 (b) presents the corresponding true stress versus true strain measurement. The conversion between nominal and true stress and strain was conducted with the usual formulae for plastically incompressible solids (we note that the material used is practically void-free).

Titanium alloys containing a high volume fraction of the low temperature HCP α-phase typically display tension–compression yield strength asymmetry when subjected to uniaxial loading conditions at room temperature [21,22]. Previous studies have investigated the yield behaviour of commercially pure titanium of various purity grades and found that the tension–compression strength asymmetry is dependent on oxygen content and crystal-

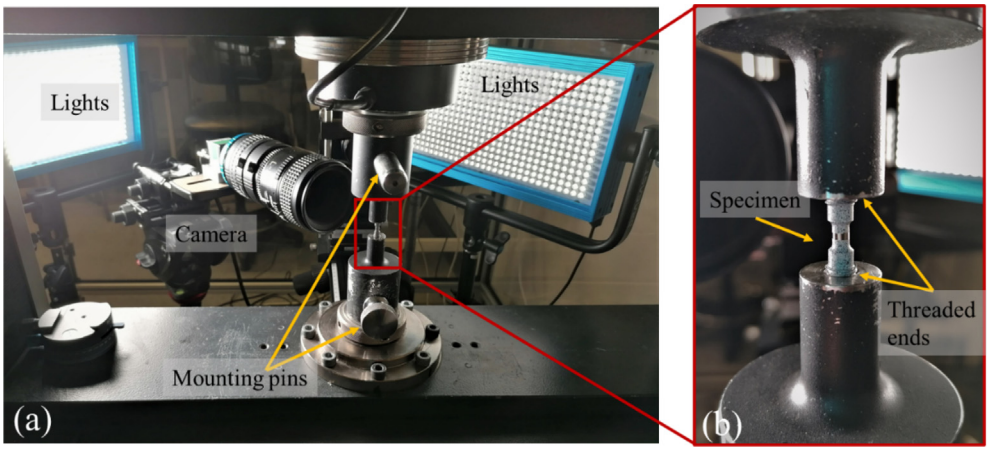

Fig. 2. (a) View of the experimental setup; (b) close-up of the specimen and loading fixtures.

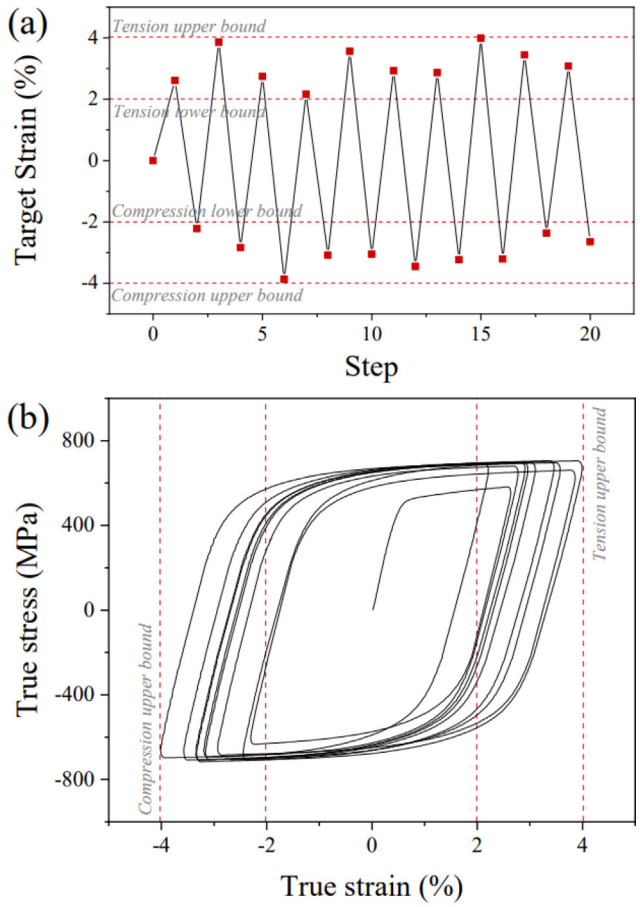

Fig. 3. (a) Example of a random imposed nominal strain history; (b) stress-strain behaviour measured during the corresponding random cyclic loading experiment.

lite orientation distribution with respect to the loading axis [21], it is therefore not present in all grades of pure titanium. Titanium samples manufacture from unidirectionally rolled plates show an appreciable tension compression yield strength asymmetry only in transverse direction [21,23]. The experimental data, obtained from samples made from an extruded bar, as expected displayed a stress versus strain response characterised by a Young's modulus of approximately 105 GPa, an initially approximately symmetric initial yield stress (the proof stress at a plastic strain of 0.2 % was approximately 520 MPa in both tension and compression), and a noticeable Bauschinger effect upon reversed plasticity.

3. Implementation of the surrogate model

3.1. Training data set

Two of the nine experiments conducted (one starting with tensile loading and one with compressive loading) were stored to perform a validation of the predictions of our surrogate model; these are indicated as "Validation set" 1 and 2 in Fig. 4. The remaining 7 experiments were used to assemble a training dataset. All data are visualised in Fig. 4, with the 7 experiments used for training shown in grey and the 2 tests for validation shown in red and blue. The corresponding time histories of strain and stress to the data in Fig. 4 are provided in Section 4. The stress versus strain measurements were used without further manipulations, with two exceptions: (i) not all recorded datapoints were used, but only 1/8 of the total were stored, as this number was sufficient to construct an accurate surrogate model; (ii) we removed the portions of the curves in the region $|\sigma| < 5$ MPa (σ is the applied stress) to elimi-

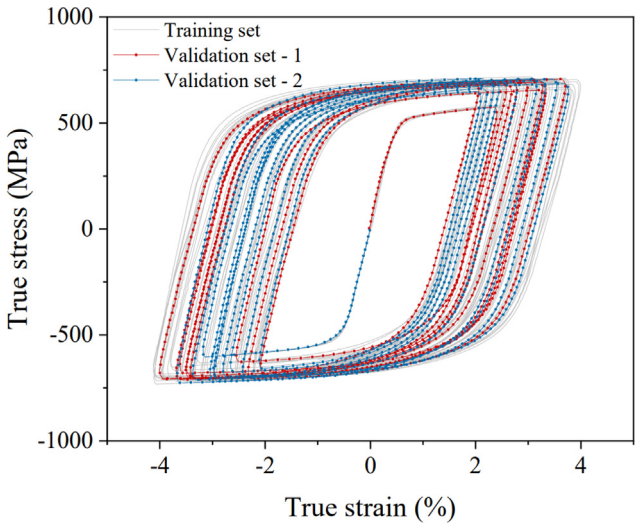

Fig. 4. A summary of the data used in this study. The measurements used for training and testing are shown in grey; the experiments used for validation are in red and blue. Only 20% of the datapoints is shown for clarity. (For interpretation of the references to colour in this figure legend, the reader is referred to the web version of this article.)

nate noisy stress/strain measurements due to the a small slack in the loading fixture. The data comprised 36,457 increments, intended as portions of the loading and deformation history spanning the time comprised between two selected measurements; each increment, or more precisely the set of values of all variables at the beginning and end of the increment, represents one point of the training dataset.

In the implementation of the surrogate model, we assume that no damage (loss of stiffness) occurs during the tests. This is partially based on the existing literature on low-cycle fatigue of commercially pure titanium [24–27], some of which shows negligible degradation of the material after 20 loading steps of strain amplitude up to 2.4 %. To assess the likelihood of fatigue damage at higher strains (up to 4 % was applied in this study), we measured the slope of the elastic unloading in our experiments, to assess the possible degradation of material stiffness. An example of such data is shown in Fig. 5 for one selected experiment. It is observed that there is no evident degradation of the Young's modulus. Its variation, of at most 5 % from step to step, is likely due to the experimental errors caused by the limited resolution of the video strain extensometer used.

3.2. Surrogate model

A feed-forward regression neural network (NN_R) [28] is used in this study to implement the surrogate model. The network performs, at every increment, the regression

$$\Delta\sigma = NN_R\left(\Delta\varepsilon, \varepsilon, \varepsilon_{el}, \bar{\varepsilon}_{pl}, \varepsilon_{\max}, \varepsilon_{\min}, \varepsilon_{last}\right) \quad (2)$$

The variation of stress across one increment is taken to be a function of the increment in total strain $\Delta\varepsilon$, the total strain ε at the beginning of the increment, the elastic strain ε_{el} at the beginning of the increment (this is equivalent to the initial stress, as $\sigma = E\varepsilon_{el}$), the accumulated plastic strain $\bar{\varepsilon}^{pl}$, quantifying the extent of plastic deformation accumulated up to the current increment, and the additional parameters $\varepsilon_{\max}, \varepsilon_{\min}, \varepsilon_{last}$, quantifying the shift of the yield surface due to the history of plastic strains experienced.

The von Mises equivalent plastic strain reduces to the axial plastic strain in a uniaxial test; therefore the accumulated plastic strain can be calculated as the sum of the absolute values of the increments in plastic strain in each loading step, i.e. $\bar{\varepsilon}_{pl} = \sum|\Delta\varepsilon_{pl}|$, where $\varepsilon_{pl} = \varepsilon - \varepsilon_{el}$, assuming additive strain decomposition.

The parameter $\varepsilon_{\max}$ is defined as the largest total tensile strain experienced by the material at the beginning of the current increment; it aims at quantifying the largest tensile plastic strain applied to the solid in its past deformation. Similarly, $\varepsilon_{\min}$ is the largest compressive strain experienced by the material at the beginning of the current increment; it has similar function as $\varepsilon_{\max}$ but focuses on compressive plastic strains. The parameter ε_{last} is defined, at any given point, as the total strain when the sign of $\Delta\varepsilon$ was last changed, i.e. when the direction of deformation was last reversed. Note that ε_{last} may or may not coincide with one between $\varepsilon_{\max}$ or $\varepsilon_{\min}$, but it cannot exceed (in absolute value) neither $\varepsilon_{\max}$ nor $\varepsilon_{\min}$. If ε_{last} does not coincide with $\varepsilon_{\max}$ or $\varepsilon_{\min}$, this indicates that the last time the deformation was reversed, the yield surface had not been shifted (or equivalently, $\varepsilon_{\max}$ or $\varepsilon_{\min}$ had not changed). Fig. 6 illustrates the evolution in time of some of the inputs of the NN eq.(2), for the same experiment shown in Fig. 3.

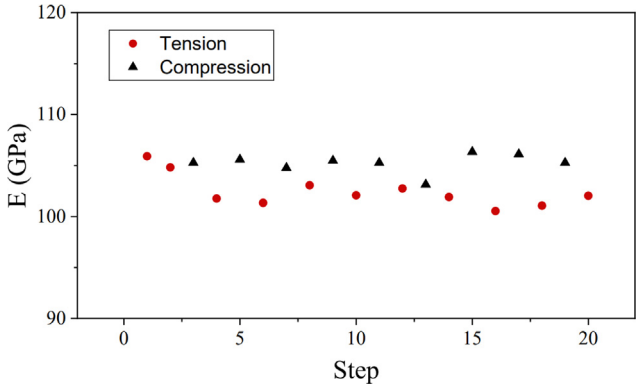

Fig. 5. Evolution of the material's Young's modulus with increasing number of loading steps, for a selected experiment.

The architecture of the NN was determined by trial and error; the final network comprised 2 hidden layers containing 100 neurons each. The inputs and outputs were rescaled to values between 0 and 1 using the minmax() function [29]; the ReLU [30] function was chosen as the activation function for the hidden layers, while the identity function was used for the output layer (i.e. no activation). The chosen loss function was the mean absolute error (MAE) [29]. The NN was trained in TensorFlow 2.0 [31] via backpropagation, using the Adam optimiser [32] with a learning rate of 0.001. The number of epochs was set to 3,000, with a batch size of 35. The data collected from the experiments shown in grey in Fig. 4 was split into two subsets; one subset contained 90 % of the total number of datapoints (increments) and was used for training, while the remaining datapoints (10 % of the total) were used for testing; the increments in the two sets were randomly selected. At the end of the training, the explained variance score [29] was found to be equal to 0.996 (out of a maximum of 1 for a perfect regression).

3.3. Assessment of the accuracy of the surrogate model

To test the fidelity of the surrogate model, We focus on the data recorded in the 2 experiments shown in red and blue in Fig. 4; these were processed as the remaining experiments, providing two strain histories, each split in sequences of consecutive applied strain increments. The surrogate model was used to predict the stress versus strain responses corresponding to these two strain histories. For each history, starting from the initial stress- and strain-free configuration ($\varepsilon = \sigma = 0$), the sequence of consecutive strain increments was provided as an input to the surrogate model; in each increment, eq. (2) was used to update the stress σ, and based on this, the accumulated plastic strain. The values of $\varepsilon_{\max}, \varepsilon_{\min}, \varepsilon_{last}$ were also updated, providing the input parameters for the subsequent increment. This allowed constructing predictions of the stress histories corresponding to the two unseen strain histories.

4. Results and discussion

Fig. 7 compares the predictions of the surrogate model to the two unseen experiments, in terms of the stress versus strain response and of stress versus time response (the strain versus time histories coincide for experiments and predictions). The NN predictions are in red and blue, while the measurements are shown in black; only 20 % of the datapoints are shown for clarity of visualisation. The surrogate model is found in excellent agreement with the experiments, accurately predicting the strain hardening characteristic of the material loaded. The predictions deviate from the experiments by at most 5 %, and such discrepancies only affect small portions of the deformation histories, consistent with the notion that the accuracy of the model is not uniform in input space,

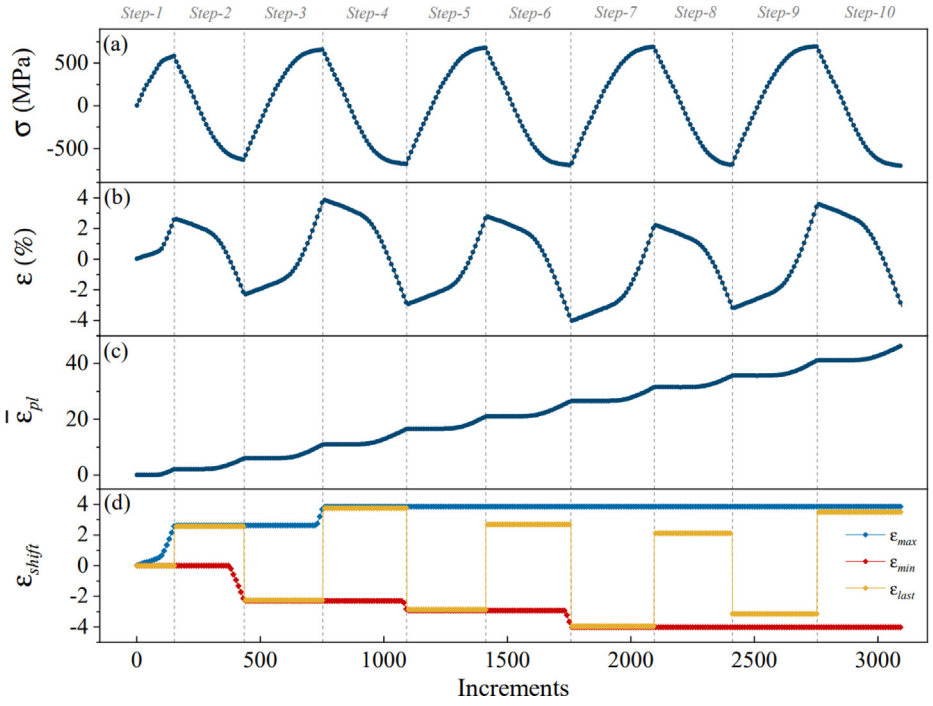

Fig. 6. The evolution of NN inputs in a selected experiment (only the first 10 steps of the experiment are shown for clarity).

which can be consequent to the non-uniform distribution of the data in input space.

Fig. 8 presents the distribution of the inputs. The comparison with experiments suggests that the proposed architecture of the surrogate model is effective in capturing the physics of the material's yielding and strain hardening. Such architecture was determined by a trial and error procedure (omitted here for brevity), which showed that the inclusion as inputs of the accumulated plastic strain $\bar{\varepsilon}^{pl}$ and of the parameters $\varepsilon_{\max}, \varepsilon_{\min}, \varepsilon_{last}$ was essential in allowing an accurate regression with a small NN and limited data. The first parameters $\bar{\varepsilon}^{pl}$ carries two types of physically relevant information: its rate $\dot{\bar{\varepsilon}}^{pl}$ allows distinguishing between elastic ($\dot{\bar{\varepsilon}}^{pl} = 0$) and elastic–plastic ($\dot{\bar{\varepsilon}}^{pl} > 0$) deformation; its magnitude quantifies the accumulated permanent changes to the material's microstructure (e.g. dislocation density). The knowledge of $\varepsilon_{\max}, \varepsilon_{\min}, \varepsilon_{last}$ provides the model with information regarding the maximum strains experienced up to the current increment, and permits determining if the current deformation follows a shift of the yield surface in the opposite direction. The size of the NN, and therefore the speed of the surrogate model, could be reduced by optimising the network's architecture and separating elastic from elastic-plastic increments, as in [2].

We note that only 7 simple uniaxial tests were required to train the data-driven model presented here, and this is comparable to the number of tests typically used to calibrate theoretical models for the response of pure titanium. Data-driven constitutive models similar to that presented here are expected to be particularly effective in the case of recently developed materials, for which there could be lack of understanding of the physical response and of corresponding theoretical descriptions. In this case surrogate models could allow immediate predictions of the response of complex components, and more rapid deployment of new materials to engineering applications.

In this study we have only explored the response of the material to deformation in uniaxial stress, therefore the surrogate predictions are only valid in such regime. For pure titanium, an extension to the case of multiaxial deformation could be attempted, by assuming and implementing appropriate constraints for a 3D surrogate constitutive model. However, for materials that are not as well understood as pure titanium, multiaxial experiments are required to assemble a suitable training dataset for a surrogate model of general applicability. The current approach assumes no damage and a rate-independent response of the material, which can be inappropriate assumptions in different strain regimes and for different solids. In our future studies we will work at overcoming the above limitations and at applying similar data-driven constitutive modelling to different materials.

To further assess the effectiveness of the surrogate model proposed, we proceed to compare its accuracy with that of a popular theoretical model for cyclic plasticity, i.e. the constitutive model proposed by Armstrong and Frederik [33] based on the von-Mises yield criterion with associative plasticity [34,35]. The above model is implemented in Abaqus [35] and can simulate non-linear isotropic and kinematic hardening in metallic alloys with a relatively modest number of hardening parameters. The evolution of the yield surface is decomposed in the isotropic part Q_{ISO}, i.e. the expansion of the yield surface, and the kinematic part Q_{KIN}, that is the shifting of the yield surface. These are functions of the accumulated plastic strain $\bar{\varepsilon}_{pl}$, as it follows:

$$\begin{aligned} \sigma_{ISO} &= Q_{\inf}\left(1 - e^{(-b.\bar{\varepsilon}_{pl})}\right) \\ \sigma_{KIN} &= \sigma_{KIN_1} + \sigma_{KIN_2} = \sum_{i=1,2} \frac{C_i}{\gamma_i}\left(1 - e^{-\gamma.\bar{\varepsilon}_{pl}}\right) \end{aligned} \tag{3}$$

where $Q_{\inf}$ denotes the maximum magnitude of the yield surface expansion and b is a parameter that controls the rate of expansion. The kinematic part of the nonlinear hardening, i.e. the translation of the yield surface resulting in the Bauschinger effect, was represented using two backstress tensors Q_{KIN_1} and Q_{KIN_2}, each corresponding to a component of translation of the yield surface. The use of two backstresses was found to be optimal to maximise the agreement between the model's predictions and the test

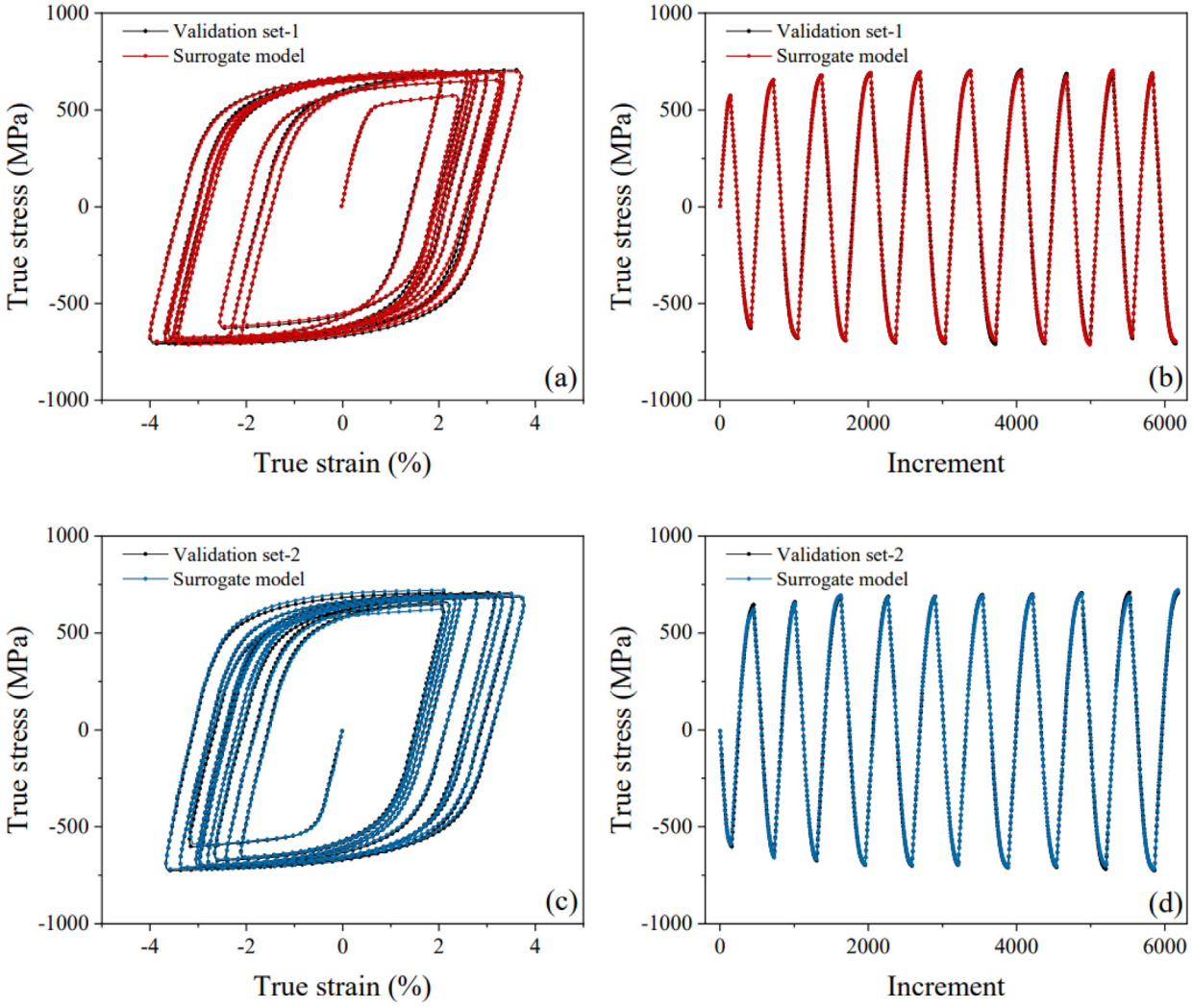

Fig. 7. Comparison between the predictions of the surrogate model and the experiments; (a, b) validation set-1; (c, d) validation set-2.

results used to calibrate the same model. The parameters C_1, C_2, and γ_1, γ_2 govern the evolution of the backstress with respect to the accumulated plastic strain. For every step of deformation, the current yield stress is equal to the sum of initial yield stress and hardening stresses due to isotropic and kinematic hardening (eq. (4), Fig. 9).

$$\sigma_y = \sigma_0 + \sigma_{ISO} + \sigma_{KIN_1} + \sigma_{KIN_2} \tag{4}$$

The parameters of the Armstrong and Frederik constitutive equation were identified using the results of additional measurements on the same material. The constitutive model required inputting the stabilised cyclic behaviour of the material in tension, as well as additional information on the variation of the yield stress during successive cycles until stabilisation. Details on the calibration of the employed combined isotropic-kinematic hardening model can be found in [35].

Additional cyclic straining experiments were conducted. The sample geometry and experimental setup were analogous to those described above, with the exception that these additional tests were conducted prescribing symmetric cycles of constant total strain amplitude (rather than a random amplitude between 0.02 and 0.04).

The experimental data, obtained from stabilised symmetric cycles, were inputted in Abaqus, which determined by optimisation the kinematic hardening parameters C_i, and γ_i. Two sets of these parameters were determined, using data from two cyclic straining experiments with different strain amplitudes of 0.02 and 0.04. Calibration parameters were determined from each experiment and then averaged to determine the set to be included in FE simulations; a summary of their value is presented in Table 1. We also note that multiple backstress terms can be considered in this model; a preliminary investigation revealed that the accuracy of the predictions is maximised when using two backstresses, therefore we make this choice in the following.

The measured stress–strain histories in these two additional cyclic tests are shown in Fig. 10, together with the corresponding predictions of the Armstrong and Frederik model.

Clearly the model fails to capture the initial yielding characteristic of the material, as such initial yielding is not part of the required inputs. It does capture reasonably well the stabilised response of the material, and it does this better in tension than in compression, as the model requires only tensile data and assumes an inherently symmetric response.

The accuracy of the proposed surrogate model is compared to that of the theoretical model [33], by testing both models when predicting the stress histories corresponding to random histories of strain. Fig. 11 illustrates such comparison. Following the first yield, the theoretical model overestimates the measured strain hardening. Upon load reversal, the theoretical model also overpredicts the stresses during the compressive yielding of the solid.

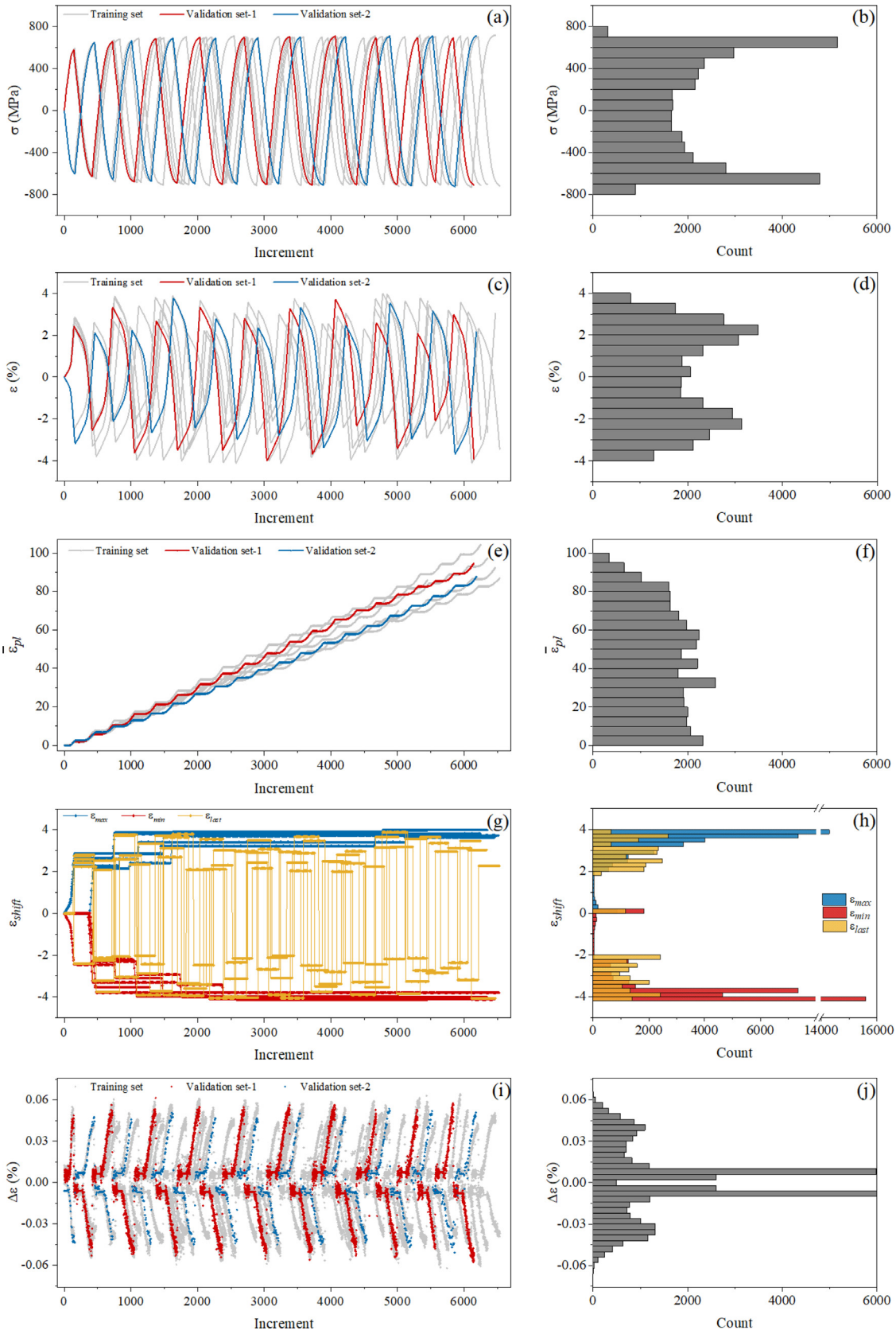

Fig. 8. Evolution in time increments and probability density distributions of (a, b) true stress, (c, d) total true strain, (e, f) accumulated plastic strain, (g, h) ε_{min}, ε_{max}, ε_{last}, and (i, j) increments of strain.

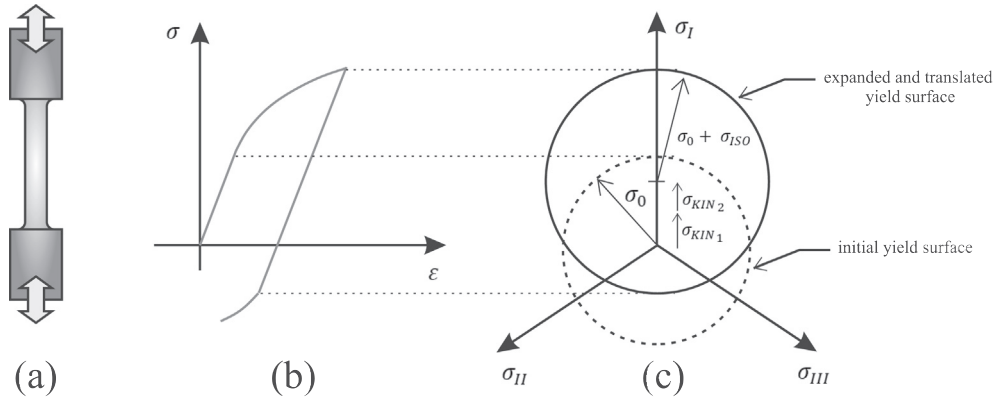

Fig. 9. Armstrong and Frederik model: (a) cyclically loaded specimen (b) stress–strain response (c) yield surface motion and expansion in the π plane.

Table 1
Kinematic/isotropic hardening model parameters.

Curve fitting of the test data					
Calibration Experiment Amplitude	Curve Fit Error	Yield Stress (MPa)	Backstress (i)	Parameter C_i (MPa)	Parameter γ_i (-)
2 %	0.00419	439.53	1	17824.	129.59
			2	100747.	1169.5
4 %	0.10236	465.89	1	4737.7	67213.
			2	67213.	407.08

Nonlinear kinematic/isotropic hardening model

Kinematic component

YieldStress (MPa)	Backstress (i)	Parameter C_i (MPa)	Parameter γ_i (-)
400.00	1	11281.	90.311
	2	83980.	788.28

Isotropic component

YieldStress (MPa)	Plastic Strain (-)
400.00	0.0000
669.55	12.601
682.71	25.347
683.99	37.933

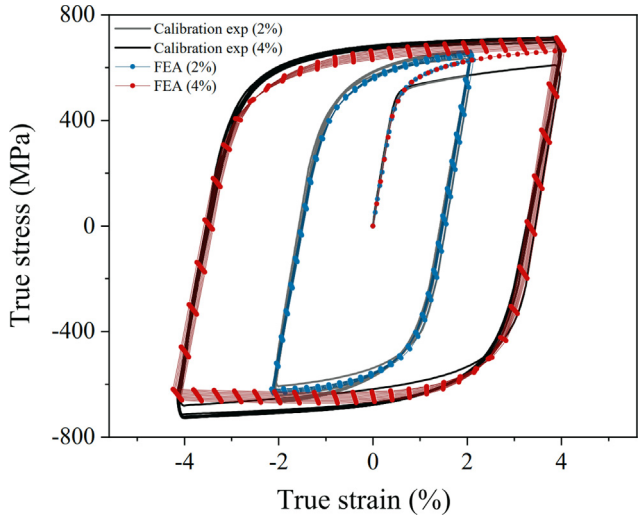

Fig. 10. Calibration experiments and predictions of the theoretical hardening model.

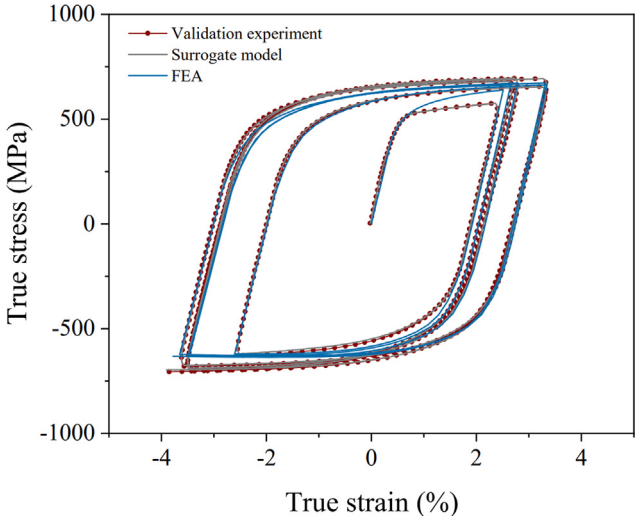

Fig. 11. Comparison of the surrogate model and the cyclic hardening model of Abaqus.

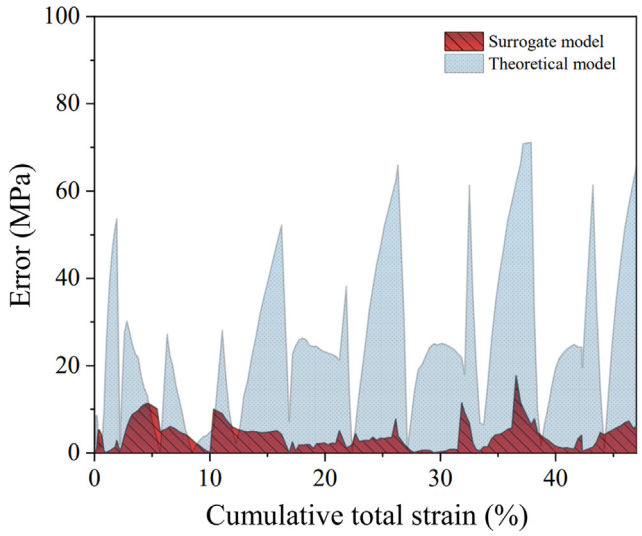

Fig. 12. Comparison of the errors of the surrogate and theoretical models.

With increasing number of random plastic straining steps, the theoretical model converges to a nearly stabilised response with smaller strain hardening than observed experimentally. The errors of the theoretical model are generally larger in compression than in tension, as the model cannot capture the asymmetric response. In contrast, the data-driven model captures all phases of the material's response.

The absolute value of the errors made by the two models at every strain increment are compared in Fig. 12. It is evident that the absolute error of the data-driven surrogate model is negligible throughout all stages of deformation, while the error of the theoretical model is initially approximately-five times larger than that of the surrogate model, and this factor tends to increase with increasing accumulated applied strain.

5. Conclusions

We presented a strategy to implement data-driven constitutive models for the uniaxial response of pure titanium. We used the results of seven experiments to train a surrogate constitutive model of the material response to random strain histories in uniaxial stress; such model predicts the change in stress over an increment of the imposed deformation. The predictions of the surrogate model were found to be computationally efficient, relying on a small feed-forward NN while achieving great accuracy. The complex yielding and strain hardening of pure titanium were captured correctly by including in the surrogate model specific inputs describing the effects of the past history of deformation, namely the accumulated plastic strain, quantifying the extent of the magnitude of past plastic deformation, and three additional parameters measuring the shift of the yield surface and the occurrence of reversed plasticity. The performance of the surrogate model was found to largely exceed that of an established theoretical model for the cyclic hardening of metals. The current approach is limited to the response of pure titanium in uniaxial stress and it assumes no loss of cohesion of the material and a rate independent response; we will explore the extension to the multiaxial response of general solids in our future studies.

Author contributions

BT conducted all experiments and machine learning activities, and wrote the first draft of the manuscript. VT proposed and planned the research, co-supervised BT and wrote the final version of the paper. AP funded, planned and supervised all experiments, supervised the experimental and modelling work of BT, edited and revised the paper.

Data availability

Data will be made available on request.

Declaration of Competing Interest

The authors declare that they have no known competing financial interests or personal relationships that could have appeared to influence the work reported in this paper.

Acknowledgements

We acknowledge funding from the Ministry of National Education of the Republic of Turkey, supporting the PhD research of Burcu Tasdemir.

References

[1] M. Mozaffar, R. Bostanabad, W. Chen, K. Ehmann, J. Cao, M.A. Bessa, Deep learning predicts path-dependent plasticity, Proc. Natl. Acad. Sci. 116 (52) (2019) 26414–26420.
[2] W. Ge, V.L. Tagarielli, A computational framework to establish data-driven constitutive models for time- or path-dependent heterogeneous solids, Sci. Rep. 11 (15916) (2021).
[3] F. Ghavamian, A. Simone, Accelerating multiscale finite element simulations of history-dependent materials using a recurrent neural network 357 (2019) 112594.
[4] B. Tasdemir, A. Pellegrino, V. Tagarielli, A strategy to formulate data-driven constitutive models from random multiaxial experiments, Sci. Rep. 12 (22248) (2022).
[5] M. Dahlberg, P. Segle, Evaluation of models for cyclic plastic deformation – A literature study, Technical Report no, Sweedish Radiation Safety Autority, 2010, p. 45.
[6] S.K. Paul, S. Sivaprasad, S. Dhar, S. Tarafder, Key issues in cyclic plastic deformation: experimentation, Mech. Mater. 43 (11) (2011) 705–720.
[7] M.A.S. Matos, S.T. Pinho, V.L. Tagarielli, Application of machine learning to predict the multiaxial strain-sensing response of CNT-polymer composites, Carbon 146 (2019) 265–275.
[8] M.A.S. Matos, S.T. Pinho, V.L. Tagarielli, Predictions of the electrical conductivity of composites of polymers and carbon nanotubes by an artificial neural network, Scr. Mater. 166 (2019) 112.
[9] J. Zhao, F. Wang, Parameter identification by neural network for intelligent deep drawing of axisymmetric workpieces, J. Mater. Process. Technol. 166 (3) (2005) 387–391.
[10] M.V. Pathan, S.A. Ponnusami, J. Pathan, R. Pitisongsawat, B. Erice, N. Petrinic, V. L. Tagarielli, Predictions of the mechanical properties of unidirectional fibre composites by supervised machine learning, Sci. Rep. 9 (13964) (2019) 1–10.
[11] Y.C. Lin, J. Zhang, J. Zhong, Application of neural networks to predict the elevated temperature flow behavior of a low alloy steel, Comput. Mater. Sci 43 (2008) 752–758.
[12] X. Li, C.C. Roth, D. Mohr, Machine-learning based temperature-and rate-dependent plasticity model: application to analysis of fracture experiments on DP steel, Int. J. Plast 118 (2019) 320–344.
[13] Z. Liu, Y. Hou, R. He, Y. Ye, C. Niu, J. Min, Machine learning for extending capability of mechanical characterization to improve springback prediction of a quenching and partitioning steel, J. Mater. Process. Technol. 308 (117737) (2022).
[14] D. Huang, J.N. Fuhg, C. Weißenfels, P. Wriggers, A machine learning based plasticity model using proper orthogonal decomposition, Comput. Methods Appl. Mech. Eng. 365 (2020) 113008.
[15] D.P. Jang, P. Fazily, J.W. Yoon, Machine learning-based constitutive model for J-2 plasticity, Int. J. Plast 138 (102919) (2021).
[16] M. Teranishi, Neural network constitutive model for uniaxial cyclic plasticty based on return mapping algorithm, Mech. Res. Commun. 119 (103815) (2022).
[17] X. Liu, J. He, S. Huang, Mechanistically informed artificial neural network model for discovering anisotropic path-dependent plasticity of metals, Mater. Des. 226 (111697) (2023).
[18] D. Liu, H. Yang, K.I. Elkhodary, S. Tang, W.K. Liu, X. Guo, Mechanistically informed data-driven modeling of cyclic plasticity via artificial neural networks, Comput. Methods Appl. Mech. Eng. 393 (114766) (2022).

[19] N.C. Sole, N. Petrinic, A. Pellegrino, An investigation on the Bauschinger effect in titanium alloys for aerospace applications, Strain Rate and Pressure Dependence, MSc Thesis, University of Oxford, 2021.
[20] S. Sivasubramaniam, The development of reverse loading split hopkinson pressure bar systems for the study of the dynamic bauschinger effect, DPhil Thesis, University of Oxford, 2010.
[21] M.C. Brandes, M. Baughman, M.J. Mills, J.C. Williams, The effect of oxygen and stress state on the yield behavior of commercially pure titanium, Mater. Sci. Eng. A 551 (2012) 13–18.
[22] P. Lin, Y. Hao, B. Zhang, S. Zhang, C. Chi, J. Shen, Tension-compression asymmetry in yielding and strain hardening behavior of CP-Ti at room temperature, Mater. Sci. Eng. A 707 (2017) 172–180.
[23] B. Revil-Baudard, O. Cazacu, E. Massoni, Room-temperature plastic behavior and formability of a commercially pure titanium: Mechanical characterization, modeling, and validation, Int. J. Solids Struct. 228 (2021) 111121.
[24] S. Sinha, N.P. Gurao, The role of crystallographic texture on load reversal and low cycle fatigue performance of commercially pure titanium, Mater. Sci. Eng. A 691 (2017) 100–109.
[25] Z.F. Zhang, H.C. Gu, X.L. Tan, Low-cycle fatigue behaviors of commercial-purity titanium, Mater. Sci. Eng. A 252 (1) (1998) 85–92.
[26] G. Kim, S.A.A. Shams, J.N. Kim, J.W. Won, S.W. Choi, J.K. Hong, C.S. Lee, Enhancing low-cycle fatigue life of commercially-pure Ti by deformation at cryogenic temperature, Mater. Sci. Eng. A 803 (2021) 140698.
[27] C.Q. Chenand, S.X. Li, Tensile and low-cycle fatigue behaviors of commercially pure titanium containing γ hydrides, Mater. Sci. Eng. A 387 (2004) 470–475.
[28] I. Goodfellow, Y. Bengio, A. Courville, Deep Learning, Press, The M.I.T, 2016.
[29] F. Pedregosa, G. Varoquaux, A. Gramfort, V. Michel, B. Thirion, O. Grisel, M. Blondel, P. Prettenhofer, R. Weiss, V. Dubourg, J. Vanderplas, A. Passos, D. Cournapeau, M. Brucher, M. Perrot, É. Duchesnay, Scikit-learn: Machine Learning in Python, J. Mach. Learn. Res. 12 (2011) 2825–2830.
[30] C. Nwankpa,W. Ijomah, A. Gachagan, S. Marshall, Activation functions: Comparison of trends in practice and research for deep learning, arXiv preprint arXiv:1811.03378, 2018.
[31] P. Singh, A. Manure, Introduction to TensorFlow 2.0, in: Learn TensorFlow 2.0, Apress, Berkeley, CA, 2020, pp. 1–24.
[32] D.P. Kingma, J.L. Ba, Adam: A method for stochastic optimization, ICLR 1412 (6980) (2015) 2014.
[33] C.O. Frederick, P.J. Armstrong, A mathematical representation of the multiaxial Bauschinger effect, Mater. High Temp. 24 (1) (2007) 1–26.
[34] R.J. Cooke, A.M. Kanvinde, Constitutive parameter calibration for structural steel: Non-uniqueness and loss of accuracy, J. Constr. Steel Res. 114 (2015) 394–404.
[35] ABAQUS, ABAQUS/Standard User's Manual, version 6.14,Desault Systems, Providence (RI, USA) (2014).